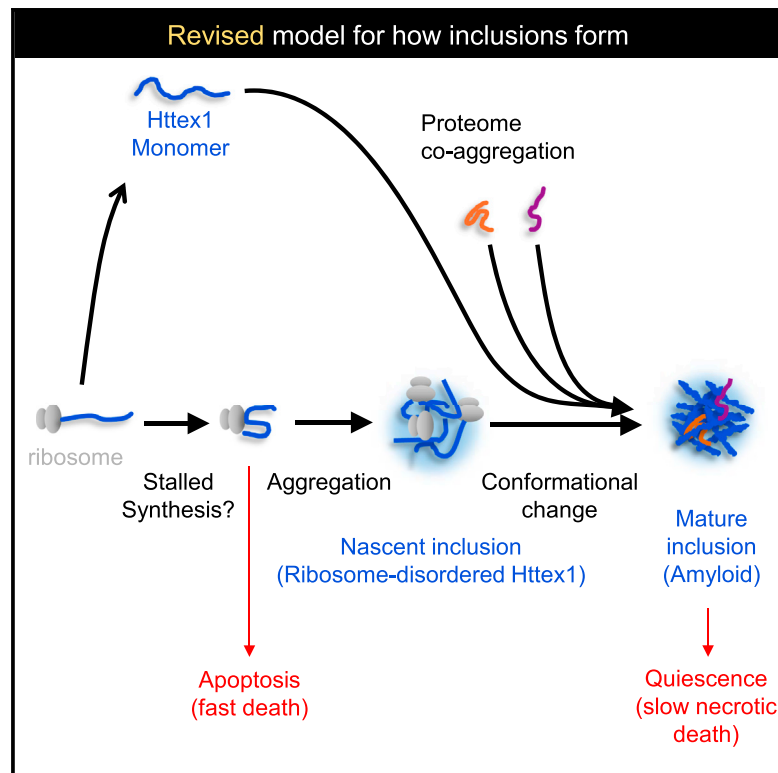


Huntingtin Inclusions Trigger Cellular Quiescence, Deactivate Apoptosis, and Lead to Delayed Necrosis

Graphical Abstract



Authors

Yasmin M. Ramdzan,
Mikhail M. Trubetskov,
Angelique R. Ormsby, ..., David B. Ascher,
Gavin E. Reid, Danny M. Hatters

Correspondence

dhatters@unimelb.edu.au

In Brief

Httex1 aggregation into inclusions has paradoxically been reported as either toxic or beneficial in Huntington's disease. Ramdzan et al. define a dual mechanism of toxicity that explains this paradox. Soluble Httex1 triggers a fast death by apoptosis, whereas Httex1 inclusions invoke quiescence and redirect death to a slower necrotic pathway.

Highlights

- Soluble mutant Huntingtin exon 1 (Httex1) triggers apoptosis
- Httex1 inclusions deactivate apoptosis but activate delayed necrosis
- Nascent inclusions form from disordered Httex1 and ribosomes
- Upon maturation, Httex1 converts into amyloid and co-recruits prion domain proteins

Accession Numbers

PXD005120



Huntingtin Inclusions Trigger Cellular Quiescence, Deactivate Apoptosis, and Lead to Delayed Necrosis

Yasmin M. Ramdzan,^{1,14} Mikhail M. Trubetskov,^{1,14} Angelique R. Ormsby,¹ Estella A. Newcombe,¹ Xiaojing Sui,¹ Mark J. Tobin,² Marie N. Bongiovanni,³ Sally L. Gras,⁴ Grant Dewson,^{5,6} Jason M.L. Miller,⁷ Steven Finkbeiner,⁸ Nagaraj S. Moily,¹ Jonathan Niclis,⁹ Clare L. Parish,⁹ Anthony W. Purcell,¹⁰ Michael J. Baker,¹ Jacqueline A. Wilce,¹⁰ Saboor Waris,¹⁰ Diana Stojanovski,¹ Till Böcking,¹¹ Ching-Seng Ang,¹² David B. Ascher,¹ Gavin E. Reid,^{1,13} and Danny M. Hatters^{1,15,*}

¹Department of Biochemistry and Molecular Biology and Bio21 Molecular Science and Biotechnology Institute, The University of Melbourne, Melbourne, VIC 3010, Australia

²Australian Synchrotron, 800 Blackburn Road, Clayton, VIC 3168, Australia

³Department of Chemistry, University of Cambridge, Cambridge CB2 1EW, UK

⁴Department of Chemical and Biomolecular Engineering and Bio21 Molecular Science and Biotechnology Institute, The University of Melbourne, Melbourne, VIC 3010, Australia

⁵Walter and Eliza Hall Institute of Medical Research, 1G Royal Parade, Parkville, VIC 3052, Australia

⁶Department of Medical Biology, University of Melbourne, Parkville, Melbourne, VIC 3010, Australia

⁷University of Michigan Kellogg Eye Center, 1000 Wall Street, Ann Arbor, MI 48105, USA

⁸Gladstone Institute of Neurological Disease, 1650 Owens Street, San Francisco, CA 94158-2261, USA

⁹The Florey Institute of Neuroscience and Mental Health, The University of Melbourne, Parkville, VIC 3010, Australia

¹⁰Monash Biomedicine Discovery Institute and Department of Biochemistry and Molecular Biology, Monash University, Clayton, VIC 3800, Australia

¹¹School of Medical Sciences, The University of New South Wales, Sydney, NSW 2052, Australia

¹²Bio21 Mass Spectrometry and Proteomics Facility, The University of Melbourne, Melbourne, VIC 3010, Australia

¹³School of Chemistry, The University of Melbourne, Melbourne, VIC 3010, Australia

¹⁴These authors contributed equally

¹⁵Lead Contact

*Correspondence: dhatters@unimelb.edu.au
<http://dx.doi.org/10.1016/j.celrep.2017.04.029>

SUMMARY

Competing models exist in the literature for the relationship between mutant Huntingtin exon 1 (Httex1) inclusion formation and toxicity. In one, inclusions are adaptive by sequestering the proteotoxicity of soluble Httex1. In the other, inclusions compromise cellular activity as a result of proteome co-aggregation. Using a biosensor of Httex1 conformation in mammalian cell models, we discovered a mechanism that reconciles these competing models. Newly formed inclusions were composed of disordered Httex1 and ribonucleoproteins. As inclusions matured, Httex1 reconfigured into amyloid, and other glutamine-rich and prion domain-containing proteins were recruited. Soluble Httex1 caused a hyperpolarized mitochondrial membrane potential, increased reactive oxygen species, and promoted apoptosis. Inclusion formation triggered a collapsed mitochondrial potential, cellular quiescence, and deactivated apoptosis. We propose a revised model where sequestration of soluble Httex1 inclusions can remove the trigger for apoptosis but also co-aggregate other proteins, which curtails cellular metabolism and leads to a slow death by necrosis.

INTRODUCTION

Huntington's disease (HD) is caused by dominant CAG trinucleotide expansion mutations in the *HTT* gene (MacDonald et al., 1993). These mutations encode an abnormally long polyglutamine (polyQ) sequence in the Huntingtin (Htt) protein, which causes its aggregation into amyloid-like fibrils (Scherzinger et al., 1999). Aggregation of N-terminal Htt fragments into intracellular inclusions is one of the key molecular signatures of HD (DiFiglia et al., 1997; Scherzinger et al., 1997). Despite this, the role of aggregation in toxicity is unclear. Aggregates, in particular soluble oligomers, have been reported to be proteotoxic (Lajoie and Snapp, 2010; Leitman et al., 2013; Nucifora et al., 2012; Takahashi et al., 2008). Aggregates may also be toxic by sequestration of critical factors required for normal growth and viability, such as transcription factors (Schaffar et al., 2004), chaperones (Park et al., 2013), and nuclear-cytoplasmic transport machinery (Woerner et al., 2016). Inclusions may also arise from (or cause) a more general collapse of proteostasis (Gidalevitz et al., 2006).

Seemingly paradoxical to the hypothesis that aggregation correlates with toxicity are data showing that formation of inclusions improves survival odds (Arrasate et al., 2004; Bodner et al., 2006). This has led to the alternative hypothesis that inclusions are formed to sequester dispersed low-oligomeric states of Httex1 and, hence, protect the cell from their harmful effects. However, the mechanisms that can reconcile the observations underpinning these two seemingly contrasting hypotheses remain unknown.

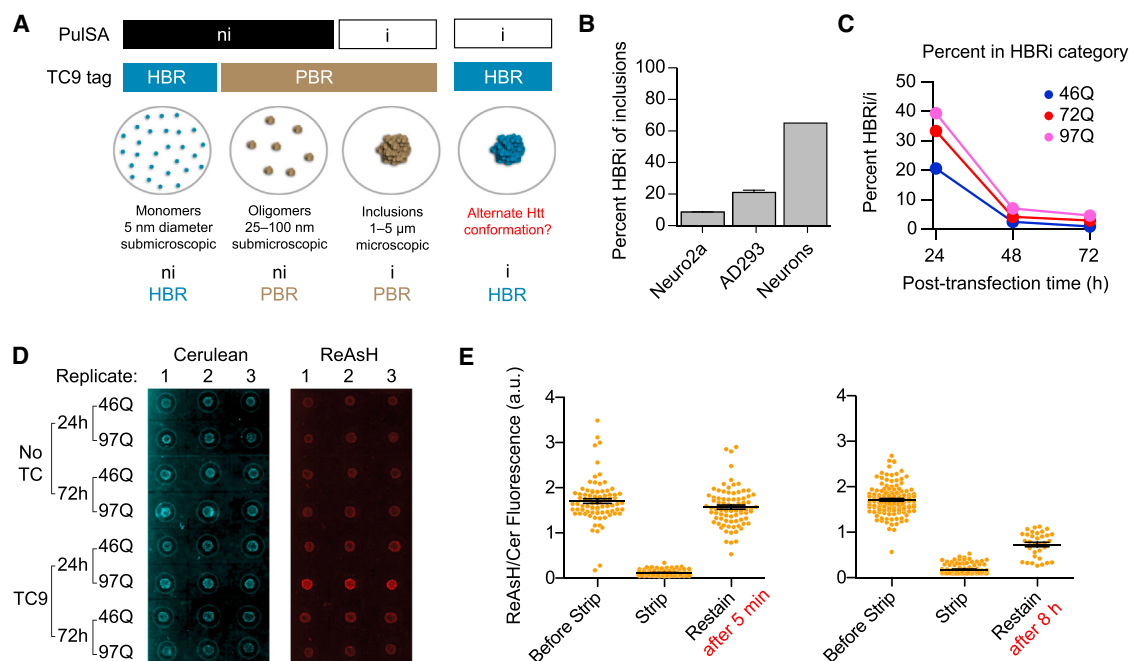


Figure 1. Formation of the HBRI and PBRI Subclasses

(A) Flow cytometry gating strategy. Collective classification of HBR and i denote an unexpected population in the cell.
 (B) Formation of HBRI in three different cell types expressing Httex1^{TC9}(97Q)-Cerulean as assessed by confocal imaging. Cortical neurons were differentiated from human embryonic stem cells and stained for ReAsH 5 days after lentiviral transduction of the construct. Neuro2a and AD293 cells were stained 24 hr post-transfection.
 (C) Formation of the HBRI class of inclusions in AD293 cells transfected with Httex1^{TC9}-Cerulean of the indicated polyQ lengths, measured by flow cytometry.
 (D) Native slot blots of insoluble fractions of Neuro2a cell lysates harvested at the indicated time points after transfection and after ReAsH staining.
 (E) Inclusions lose biarsenical reactivity over time. Plated AD293 cells were stained with ReAsH 24 hr after transfection with Httex1^{TC9}(97Q)-Cerulean and stripped of ReAsH with BAL treatment. Cells were restained with ReAsH after culturing for a further 5 min or 8 hr. Means and SEM are shown.

Using a biosensor of the Httex1 conformational state, we unearthed two types of inclusions that earmark early and late stages of the inclusion-building process. Investigation of how these inclusions form and relate to the broader homeostatic state of the cell led us to find that inclusion assembly deactivated a heightened risk of apoptosis triggered by soluble mutant Httex1 but, in doing so, initiated a cellular quiescence that led to a slower death by necrosis.

RESULTS

Detection of Early-Formed and Late-Formed Subclasses of Inclusions Formed by Htt Exon 1: HBRI and PBRI

We previously created a biosensor derivative of Httex1, Httex1^{TC9}, that reported on whether the protein was monomeric or in an amyloid conformation through a two-color fluorescence detection scheme (Ramdzan et al., 2010). Conformation was read out by reactivity of engineered tetracysteine tags to the biarsenical dyes 4,6-*bis*(1,3,2-dithiarsolan-2-yl)-7-hydroxy-3H-phenoxazin-3-one (ReAsH) or 4',5'-*bis*(1,3,2-dithiarsolan-2-yl)-3',6'-dihydroxy-spiro[isobenzofuran-1(3H),9'-[9H]xanthen]-3-one (FIAsH), which efficiently bind to the biosensor (highly biarsenically reactive [HBR]) when the tag is accessible in the

monomeric, disordered state but do not bind (poorly biarsenically reactive [PBR]) when it is inaccessible in the β sheet-rich amyloid fibril state (Ramdzan et al., 2010). Protein localization was tracked by a Cerulean fluorescent protein tag as the second color channel. We also devised a protocol to rapidly screen cells for localization of the Cerulean tag by a flow cytometry method (pulse shape analysis [PuISA]), which distinguishes cells with inclusions (i) from those with only diffuse Httex1 (no inclusions, ni) (Ramdzan et al., 2012). The use of the biosensor and PuISA together enabled us to distinguish three key groups of cells: cells enriched with Httex1^{TC9} monomers (HBRni), oligomers (PBRni), or inclusions (PBRI) (Figure 1A).

The Httex1^{TC9} biosensor was originally developed using polyQ lengths of 25Q (non-aggregating) or 46Q (aggregating) and applied in the Neuro2a cell line (Ramdzan et al., 2012). When we examined Httex1^{TC9} in other cell lines and with longer polyQ lengths, some of the cells with inclusions displayed high biarsenical reactivity, which we designated as the HBRI population (Figure 1B; see Figures S1A and S1B for further details on expression levels and aggregation extent). The proportion of HBRI cells in cells with inclusions decreased with time, suggesting that biarsenical reactivity is a transient property of cells with inclusions (Figure 1C). Native slot blots of the insoluble fraction

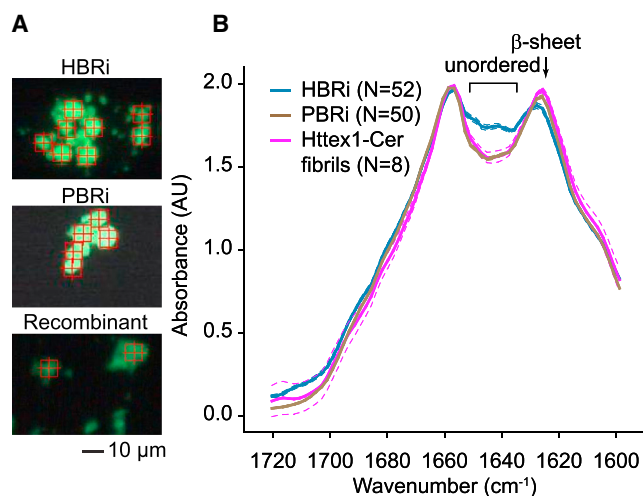


Figure 2. Httex1 Is Disordered in Early-Formed Inclusions and Converts to Amyloid over Time

(A) Fluorescence micrograph of inclusions and amyloid fibrils formed by purified Httex1-Cerulean for FTIR analysis (red cross-hairs mark representative beam clipping windows).

(B) Mean FTIR spectra with replicates referring to individual inclusions. Solid lines show means, and dashed lines show SEM.

of whole-cell lysate labeled with ReAsH at different time points after transfection supported this conclusion (Figure 1D). In addition, HBRi-categorized cells were proportionally more abundant at lower expression levels (Figure S1C) and had smaller inclusions (Figure S1D).

These data suggested that HBRi status earmarked an earlier step in the inclusion assembly process and PBRi a more mature state. To test this hypothesis, we examined the capacity of HBRi cells to be restained with ReAsH over time. Inclusions could be stripped with ReAsH using a non-toxic reducing agent (British anti-Lewisite [BAL]) and fully restained after 5 min (Figure 1E). However, staining after 8 hr led to a significant reduction in reactivity, consistent with a conversion to PBRi status (Figure 1E).

For clues to why Httex1 adopts an aggregated state permissive to biarsenical reactivity in HBRi inclusions, we examined the protein secondary structure of purified individual inclusions using synchrotron Fourier transform infrared (FTIR) microscopy (Figure 2A; Figures S2A and S2B). The amide I spectra of inclusions of the PBRi category on average matched those of recombinant Httex1-Cerulean amyloid fibrils, consistent with a notable β sheet signal ($\sim 1626\text{ cm}^{-1}$) (Figure 2B; Figure S3A). By contrast, HBRi-categorized inclusions on average substantially differed to PBRi with less β sheet and greater disordered structure (Figure 2B; Figure S3A). The HBRis were also more heterogeneous than PBRi inclusions (Figure S3A). Multivariate analysis indicated that HBRis formed a continuum of states that, on one end, consisted of disordered structure and, on the other end, were more similar to the PBRi state (Figure S3B). These data suggested that biarsenical reactivity in the HBRi state arises from the accumulation of non-amyloid disordered structure, whereby the

tetracysteine tag remains solvent-accessible (in contrast to the amyloid conformation).

Inclusion Formation Suppresses Apoptosis and Leads to a Delayed Necrosis

During our time-lapse imaging analysis, we noticed that just over half of the cells labeled as PBRi at 24 hr died non-apoptotically, whereas those retaining diffuse Httex1 or earmarked as HBRi (at 24 hr) died almost entirely by apoptosis (Figure 3A; details on how we classified the cells by microscopy are shown in Figure S4). This result led us to speculate that inclusion formation deactivated a risk of apoptosis arising from the soluble Httex1 forms.

To test this hypothesis, we first applied a broad-spectrum caspase inhibitor, (3S)-5-(2,6-Difluorophenoxy)-3-[[[(2S)-3-methyl-1-oxo-2-[[[2-quinolinylcarbonyl]amino]butyl]amino]-4-oxo-pentanoic acid hydrate (QVD-OPh) (Caserta et al., 2003), which both abrogated the apoptotic death (Figure 3A) and substantially increased the survival time of all cell groups (Figure 3B). We also found that when cells formed an inclusion, death by apoptosis was significantly correlated to shorter survival times than cells that died by necrosis (Figure 3C; these effects were not correlated with the expression level; Figure S5). We fitted the data in Figures 3A–3C to a simple three-state model to define the relative risks of apoptosis as inclusions form and mature. This yielded an excellent fit (correlation coefficient of 0.96) and indicated risks of apoptosis 4.8-fold higher for cells retaining soluble Httex1 versus HBRi and 8-fold higher for cells retaining soluble Httex1 versus PBRi (Figure 3D; full details of the fit can be found in Table S1).

To examine whether the origin for risk of apoptosis resided in the pool of soluble Httex1, we measured the levels of diffuse Httex1 in cells both at the time point of HBRi and PBRi classification (24 hr; Figure 3E) as well as 1 hr prior to death (Figure 3F). In both cases, the levels of soluble Httex1 were higher in cells with HBRi and in cells that die by apoptosis.

Next we developed an independent method to track early-formed inclusions and late-formed inclusions to investigate the possibility that apoptosis is triggered as an artifact of the biarsenical dyes. This involved fusing Httex1 to the fluorescent timer (FT)-fast protein, which converts blue to red fluorescence over a period of several hours (Subach et al., 2009). As inclusions formed and trapped Httex1 proteins, cells containing inclusions became progressively more red-fluorescent over time; hence, the “color” of the cells with inclusions, as measured with PulSA (or microscopy), enabled a distinction of cells with “young” inclusions from those with “old” inclusions (Figures S6A and 6B). This strategy to classify inclusions at 24 hr of expression (by microscopy) resulted in similar patterns for survival and mechanisms of death to that determined with the biarsenical dye strategy, indicating that the biarsenical dyes do not aberrantly induce apoptosis (Figures S6C and 6D).

Using the timer protein approach, we also tested whether cells with old inclusions were functionally impaired from activating apoptosis. Three pharmacological stimulants of apoptosis were able to activate apoptosis in cells with old inclusions (Figure S6D). Hence, we concluded that inclusion formation disarms

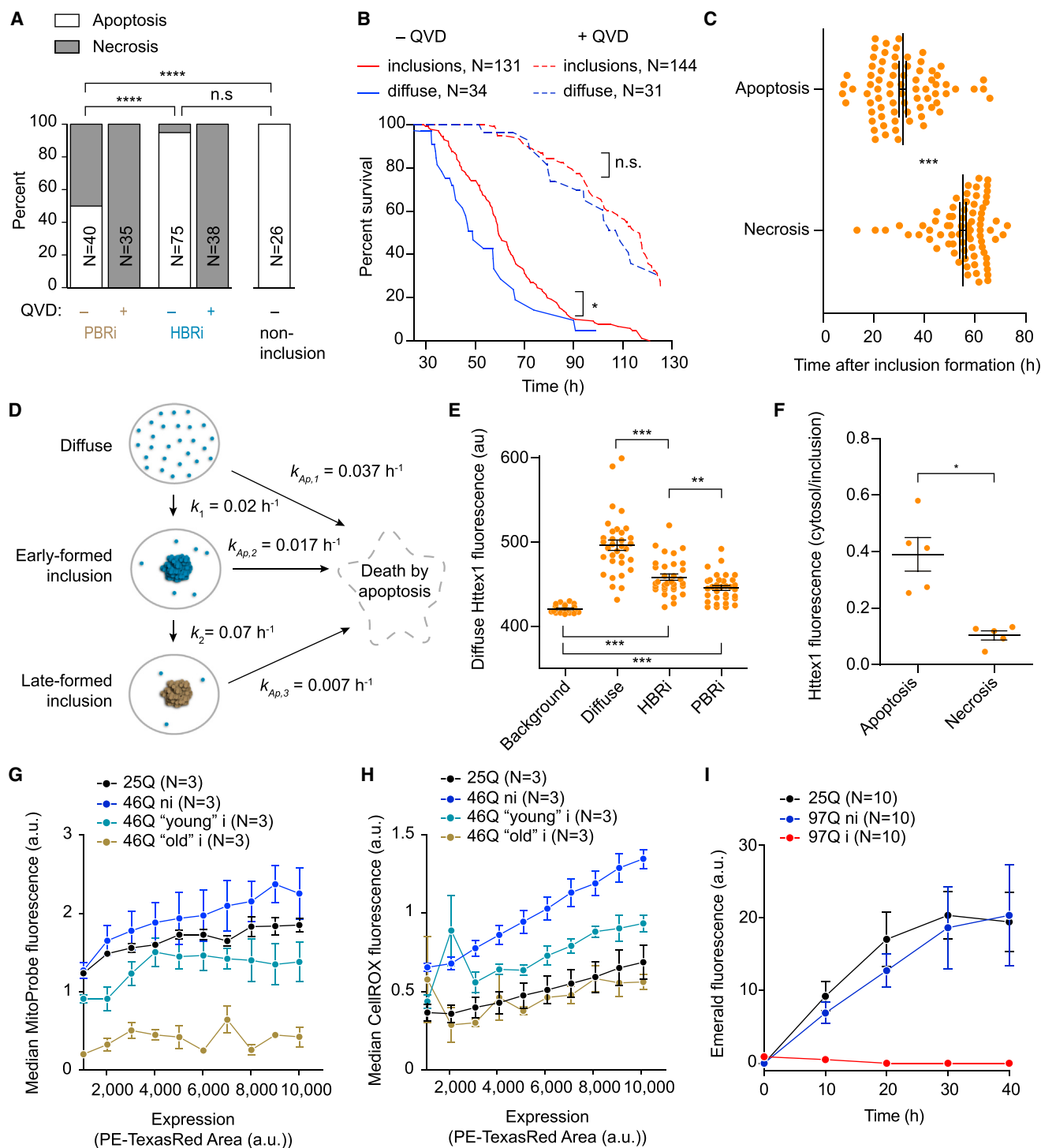


Figure 3. Inclusion Formation Disables Apoptosis, Promotes Quiescence, and Switches Death to Slow Necrosis

Shown is analysis of Httex1^{TC9}(97Q)-Cherry (or Cerulean) constructs transfected into AD293 cells. Where relevant, error bars indicate means \pm SEM.

(A) Assessment of mechanism of cell death by a live-cell caspase-3 activation assay on cells earmarked as HBri or PBRi 24 hr after transfection versus cells that die lacking inclusions. Differences were evaluated by two-tailed Fisher's exact test. QVD represents the broad-spectrum caspase inhibitor that blocks apoptosis. (B) Survival curve of cells transfected with Httex1^{TC9}(97Q)-Cerulean measured from 24 hr after transfection. Differences were assessed by survival curve analysis and Mantel-Cox test.

(legend continued on next page)

the trigger of apoptosis from soluble Httex1 forms but does not disable the apoptotic machinery.

Inclusion Formation Correlates with Functional Quiescence

To determine why apoptosis is switched off as inclusions form, we examined the metabolic state of cells. Examination of the mitochondrial membrane potential using the MitoProbe reagent (Figure 3G) indicated cells with soluble Httex1(46Q) (ni) to be hyperpolarized and for cells with inclusions to be progressively hypopolarized relative to Httex1(25Q). Hyperpolarization of the mitochondrial membrane potential enhances off-pathway production of reactive oxygen species (Korshunov et al., 1997) and is consistent with soluble Httex1 triggering a state of stress concomitant with apoptosis. Indeed, cells with soluble Httex1(46Q) had an elevated CellRox signal, and those with inclusions were restored to the baseline level of the Httex1(25Q) counterpart (Figure 3H).

The hypopolarized membrane potential of cells with old inclusions suggested a state of quiescent metabolism. Hence, as a test for quiescence, we examined the ability of cells to translate a tetracycline-inducible reporter protein (Emerald). We found that the reporter could not be induced in cells that had pre-existing Httex1(97Q) inclusions, whereas cells with diffuse Httex1 showed no difference in induction compared with the control 25Q counterpart (Figure 3I). These data suggested that inclusion formation leads the cell into a state of broad functional quiescence.

Inclusions Appear to Originate from Httex1 Emerging from the Ribosome

Next we investigated the proteins that co-aggregated with HBRI- and PBRI-classified inclusions by quantitative proteomic analysis after sorting them by flow cytometry (as shown in Figure S2).

HBRI-enriched proteins included ribosome proteins and other ribonucleoproteins (Figure 4A; Table S2). PBRI-enriched proteins included other ribonucleoproteins, especially a subset of proteins that operate mRNA splicing or processing, a cluster of chaperones, and the Httex1 protein itself (Figure 4A; Table S2). The PBRI-enriched proteins also included proteins involved in RNA stress granule biology and neurodegenerative disease (Figure 4A). This included RNA-binding protein FUS and

heterogeneous nuclear ribonucleoprotein (HNRNP) family proteins that, when mutated, cause amyotrophic lateral sclerosis (Kim et al., 2013; Vance et al., 2009). Classic components of stress granules, HSPB1 (HSP27) and PCBP1, were also enriched (Table S2; Kedersha et al., 1999). Many RNA granule proteins contain predicted prion-like domains that mediate liquid:liquid protein phase separation and/or “functional” amyloid scaffolding (Li et al., 2013). Hence, these proteins may be selectively recruited into the inclusion by a co-aggregation mechanism as Httex1 adopts an amyloid structure. Analysis of the prion domain propensity using the prion-like amino acid composition (PLAAC) algorithm (Lancaster et al., 2014) indicated that PBRI-enriched proteins were significantly more “prion-like” than a random set of proteins from the proteome (Figure 4B; Table S2). In contrast, HBRI-enriched proteins were not significantly more prion-like. A similar correlation was observed when the proteins were examined for glutamine content on the basis that polyQ-containing proteins are also able to recruit other polyQ proteins into the aggregates (Figure 4C). Of note was that several proteins enriched in the PBRI contained short stretches of glutamine-rich sequences (Table S2). To test whether prion-domain containing proteins can be recruited to the inclusions after the inclusion has initially formed, we co-expressed Httex1(97Q)-Cherry with TIA-1-GFP, a classic prion-like stress granule-associated protein that has a high PLAAC score of 22.2 and high glutamine content of 9.1% (Kedersha et al., 1999). Time-lapse images confirmed the recruitment of TIA-1 into Httex1 inclusions subsequent to Httex1 inclusion formation (Figure 4D).

DISCUSSION

Our study reconciles the large number of conflicting studies on the link between Httex1 inclusion formation and toxicity. In accord with the adaptive model of sequestration of toxic soluble Httex1 into inclusions, we showed that cells with soluble 97Q Httex1 have an elevated mitochondrial membrane potential, elevated levels of reactive oxygen species, and an elevated risk of triggering apoptosis. In accord with the model of pathogenic co-aggregation of essential cellular machinery, we showed that Httex1 inclusion formation progressively leads to a state of functional quiescence. Most importantly, our findings indicate that the prolonged survival of cells with inclusions can be explained by switching from a fast, directed death mechanism

(C) Mechanism of death on cells with respect to the length of time an inclusion has formed in cells measured by longitudinal imaging assays. Shown is mechanism of death, where apoptosis is indicated by a positive signal in the caspase-3 activation assay prior to cell lysis. The difference was evaluated by a two-tailed Student's t test.

(D) Fits of the data in (A)–(C) to the model shown. Relative rates are shown (k_{in} , rates of transition between states; $k_{Ap,n}$, rates of apoptosis where n represents the starting state).

(E) Fluorescence intensity of diffuse Httex1^{TC9}-Cerulean in cells at the time point of classification after ReAsH staining (24 hr after transfection). The differences were evaluated by two-tailed Student's t tests.

(F) Fluorescence intensity ratio of cytosolic:inclusion localized Httex1^{TC9}(97Q)-mCherry in cells with inclusions 1 hr prior to death. The differences were evaluated by two-tailed Student's t tests.

(G) Flow cytometry measurement of mitochondrial membrane potential with MitoProbe on AD293 cells 24 hr after transfection with Httex1^{TC9}-FT-fast (further gating details are shown in Figure S6).

(H) Equivalent experimental design to (G) using CellROX reagent for total cellular reactive oxygen species.

(I) Longitudinal induction of Emerald fluorescent protein expression (off a tetracycline regulatable promoter) in HeLa cells concurrently expressing Httex1^{TC9}(97Q)-Cerulean off a constitutive promoter. Time point indicates time after induction of Emerald expression by addition of tetracycline, which was 24 hr after transfection. Cells were categorized into those retaining diffuse Httex1 or inclusions upon addition of tetracycline.

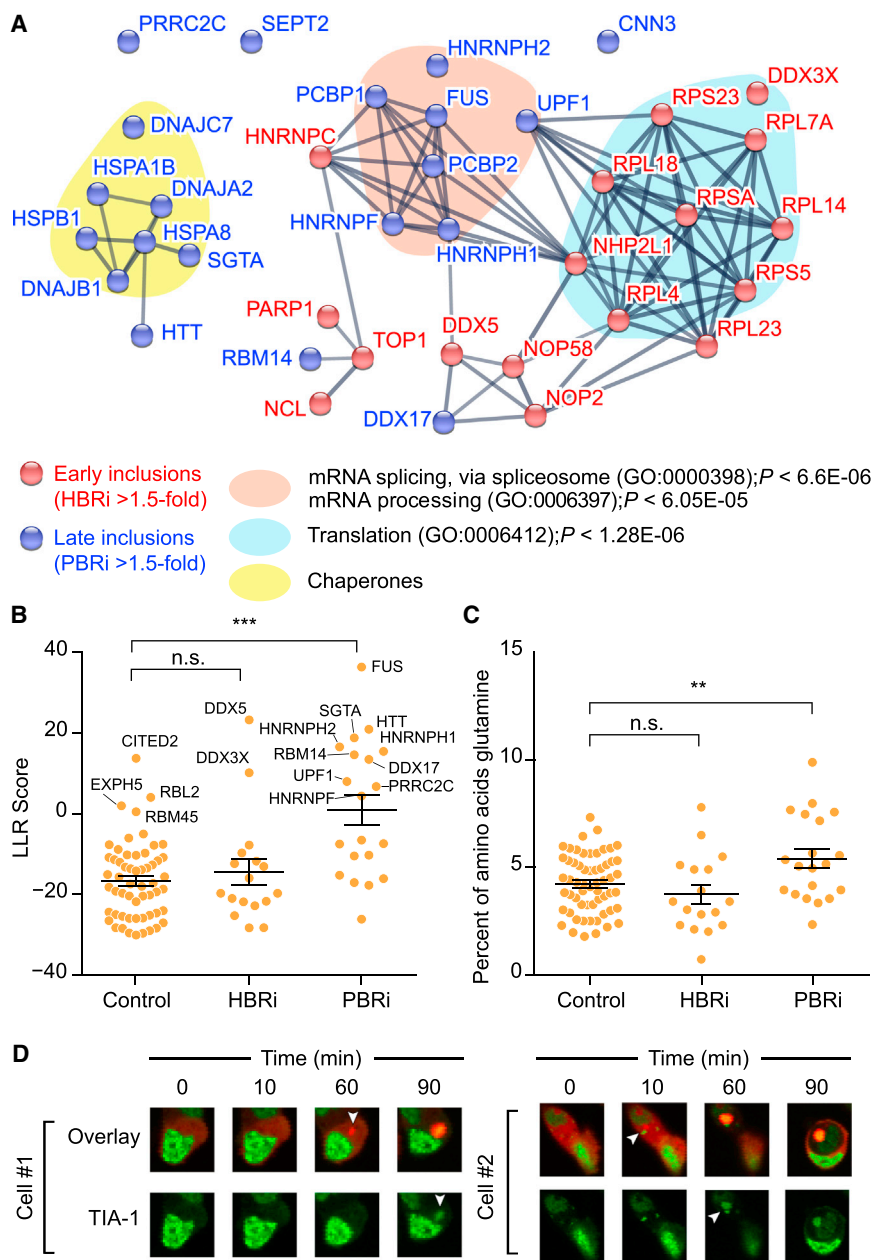


Figure 4. Early Inclusions Recruit Translational Machinery, whereas Mature Inclusions Attract Proteins with Predicted Prion-like Domains

(A) Protein-protein interaction network (STRING v10) of proteins identified in inclusions (the full list of proteins can be found in Table S2).

(B) Analysis of prion domains using the PLAAC algorithm. Higher log-likelihood ratios (LLR) relate to sequences in proteins more likely being a prion domain.

(C) Glutamine content versus control dataset of random human proteins (listed in Table S2).

(D) Recruitment of GFP-tagged prion domain protein TIA-1 (green) into Httex1(97Q)-Cherry inclusions (red) after the inclusion has formed. Two representative cells are shown in a time-lapse series.

Our data and proposed mechanism are summarized in Figure S7 (the legend of which includes an additional discussion). We postulate the presence of a quality control mechanism that clears aggregating proteins emerging from the ribosome in cells lacking inclusions. Prior data have shown that polyQ-expanded Httex1 is more efficiently degraded in cells lacking inclusions than the wild-type counterpart, which is consistent with an elevated clearance mechanism at this step (Ormsby et al., 2013; Tsvetkov et al., 2013). It follows that excessive blockage of this quality control mechanism could activate apoptosis, which provides a simple explanation for the proteotoxicity of the soluble Httex1. One candidate for this putative quality control mechanism is the ribosome quality control complex (RQC) (Brandman et al., 2012). The RQC is only beginning to be understood (in yeast) and functions to clear faulty mRNA sequences that lead to stalled ribosome-nascent protein complexes, such as non-sense-mediated

(apoptosis) to a slow, passive one (necrosis) arising from cellular quiescence.

It remains to be established whether the disarmament of apoptosis is a by-product of quiescence or part of an active strategy to suppress toxicity. Clues can be gleaned from previous findings of expression of a 97Q form of Httex1 switching off apoptosis in sympathetic neurons (from rat superior cervical ganglia) and converting death to necrosis (King et al., 2008). However, in contrast to our findings, apoptosis could not be triggered with potent proapoptotic stimuli. Hence, it remains possible that quiescence is progressive; first by disabling the trigger for apoptosis and subsequently the machinery required to execute it.

decay or no-go decay (Brandman and Hegde, 2016; Lykke-Andersen and Bennett, 2014). UPF1 (RENT1), which plays a central role in non-sense-mediated decay (Lykke-Andersen and Bennett, 2014), was enriched in PBRI, suggesting a link to a mammalian RQC counterpart mechanism. However, we did not see any of the human counterparts of the yeast RQC in our data (Ltn1, Rqc1, Cdc48, or Tae2) (Brandman and Hegde, 2016; Lykke-Andersen and Bennett, 2014), suggesting that the RQC mechanism governing clearance of polyQ-expanded Httex1 in mammalian cells is different.

The cluster of heat shock protein family chaperones enriched with late-stage inclusions may point to a delayed attempt by the cell to degrade and clear the inclusions. Others have suggested

that stress granule formation aids in the management of proteome stresses by preventing apoptosis and reducing reactive oxygen species (Arimoto et al., 2008; Takahashi et al., 2013). Hence, it remains possible that inclusion formation involves an ancillary stress granule-associated proteostatic response that represses cellular metabolism. Of note, Huntingtin fragments in the soluble state can partition with stress granules, P bodies, and translational machinery (Culver et al., 2012; Savas et al., 2010).

In conclusion, our findings have important implications in pathology. It is conceivable that neurons may exist for extended periods of time in a quiescent state *in vivo* after they form inclusions. Such neurons would be expected to be viable but functionally suppressed and, hence, could impose large contributions to the state of neurological dysfunction in the disease process before the neurons die.

EXPERIMENTAL PROCEDURES

Expanded details of the methods are listed under [Supplemental Experimental Procedures](#).

DNA Vectors and Constructs

The fluorescent proteins and human Httex1, Httex1^{TC9}, and Httex1^{TC1} as fusions to fluorescent proteins were expressed in vectors with cytomegalovirus (CMV) promoters. The gene encoding the fast fluorescent timer variant of mCherry was synthesized from the reported sequence (Subach et al., 2009). The GFP-TIA1 construct was kindly provided by Myriam Gorospe (NIA-NIH). The lentiviral vectors FUGW, psPAX2, and pCMV-VSV-G were used to generate lentiviral particles for expressing Httex1 variants.

Cell Culture

HEK293T, AD293, and HeLa cells (ATCC) were maintained in DMEM and Neuro2a in Optimem (Invitrogen). The medium was supplemented with 10% (v/v) fetal calf serum (FCS), 1 mM glutamine, and penicillin-streptomycin (pen-strep). The HeLa tet repressor line was generated with the T-REX system (Invitrogen). H9 human embryonic stem cells were induced into the neuronal lineage as described previously (Denham et al., 2012). The day 7 neurospheres were differentiated into cortical neurons using N2B27 medium supplemented with 1 μ M N-[N-(3,5-Difluorophenacetyl)-L-alanyl]-S-phenylglycine t-butyl ester (DAPT) and 20 ng/mL brain derived neurotrophic factor (BDNF).

Western Blot

AD293 cells were transfected with pT-REX-Httex1(97Q)^{TC9}-Cerulean. After 24 hr, lysates (30 μ g of cellular proteins) were subjected to western blot probed with anti-Huntingtin antibody (Abcam, ab109115).

Transfections and Transduction

Cell lines were transiently transfected with the vectors using Lipofectamine 2000 reagent (Life Technologies). Lentiviral particles were made using standard CaCl₂ transduction of HEK293T feeder cells and applied to day 7 cortical neurons. Inclusion formation was observed 5 days after lentiviral neuronal transduction.

Flow Cytometry

Cells were analyzed by PulSA with an LSRFortessa flow cytometer (BD Biosciences) as described previously (Ramdhan et al., 2012).

Confocal Imaging

Images of live or fixed cells were acquired with a Leica TCS SP5 microscope.

Slot Blot Assays

Neuro2a cells were lysed in 20 mM Tris, 2 mM MgCl₂, and 1% (w/v) Triton X-100 (pH 8.0) supplemented with cComplete EDTA-free protease inhibitor

cocktail pills (Roche) and 20 units/mL Benzonase (Novagen). The lysate was pelleted, and the insoluble fraction was resuspended in 200 μ L Platereader buffer (20 mM Tris, 150 mM NaCl, 250 μ M BAL, and 1 mM tris(2-carboxyethyl)phosphine [TCEP, pH 7.4]). ReAsH was added to 1 μ M and incubated for 30 min. Samples were filtered through a nitrocellulose membrane and washed three times in Platereader buffer. The membranes were imaged on a fluorescent scanner (Typhoon, GE Healthcare).

FTIR Microscopy and Data Processing

Inclusions were purified as described for the proteomics experiments and then pelleted and washed in water. Recombinant Httex1-Cerulean fibrils were prepared as described previously (Olshina et al., 2010) and concentrated into pellets by centrifugation (12,000 \times g, 15 min, 4°C). FTIR spectra were collected at the Infrared Microspectroscopy beamline at the Australian Synchrotron using a Bruker Hyperion 2000 IR microscope and Vertex 80v FTIR spectrometer.

ReAsH Staining, Stripping, and Restaining

For ReAsH staining, after 24 hr transfection (or transduction in the case of neurons), cells were washed twice with HBSS and stained with 1 μ M ReAsH and 10 μ M 1,2-ethanedithiol in Hank's balanced salt solution (HBSS) for 30 min at 37°C. The cells were then washed with 250 μ M BAL for 15 min at 37°C, followed by a wash with HBSS.

For the stripping and restaining experiments, AD293 cells expressing pT-REX-Httex1^{TC9}(97Q)-Cerulean were labeled with ReAsH 24 hr after transfection as described above. The cells were imaged with a JuLI-stage microscope (Nano-EnTek). ReAsH was stripped by 15-min treatment with 50 mM BAL in HBSS at 37°C followed by three washes with HBSS and then imaged again. Cells were then restained with ReAsH as described above at the time points indicated in the figures. Data were analyzed as described under [Survival Analyses](#).

Survival Analyses

AD293 cells were co-transfected with pT-REX-HttEx1^{TC9}(97Q)-Cerulean (or pT-REX-HttEx1^{TC9}(97Q)-FT-Fast) and pT-REX-mCherry (or pT-Rex-Cerulean). 24 hr after transfection, the medium was refreshed. To block caspases, QVD-OPH (50 μ M) was added at 24 hr. Cells were imaged longitudinally with a JuLI-stage fluorescence microscope (NanoEnTek). For analysis of cells assessing mechanism of death, apoptosis was measured using CellEvent caspase-3/7 green detection reagent (Life Technologies, catalog number C10423) according to the manufacturer's instructions.

AD293 cells were treated with MitoProbe DiOC₂(3) (50 nM) or CellROX (5 μ M) for 30 min in a cell culture incubator at 37°C, washed with PBS, and analyzed by flow cytometry as described previously (Ramdhan et al., 2012).

Sample Preparation for Proteomics

AD293 cells transfected with pT-REX-Httex1^{TC9}(97Q)-Cerulean were harvested 24 hr after transfection, lysed in 20 mM Tris, 2 mM MgCl₂, and 1% (w/v) Triton X-100 (pH 8.0) supplemented with cComplete EDTA-free protease inhibitor cocktail pills (Roche) and 20 units/mL Benzonase (Novagen). The lysate was subjected to flow cytometry sorting on a BD FACS Aria III instrument to separate HBRis and PBRis. Sorted inclusions were washed in PBS three times, dissolved in formic acid for 30 min, and neutralized with 3 M Tris. Samples were digested with trypsin and differentially labeled by reductive dimethylation. Samples were matched for total protein levels.

NanoESI LC-MS/MS Analysis

Samples were analyzed by nano-electrospray ionization (nanoESI) liquid chromatography-tandem mass spectrometry (LC-MS/MS) and analyzed with nanoflow reverse-phase high-performance liquid chromatography (HPLC) and analyzed according to standard quantitative proteomic workflows (see details in the [Supplemental Experimental Procedures](#)).

Bioinformatics

PLAAC analysis was performed as described previously (Lancaster et al., 2014). Glutamine content was analyzed with the statistical analysis of protein sequences (SAPS) algorithm by European Molecular Biology Laboratory (EMBL) European Bioinformatics Institute (EBI) (<http://www.ebi.ac.uk/Tools/seqstats/saps/>).

Data Modeling

The data in Figures 3A–3C were modeled using a discrete state model in R, where the cells could exist in three states (1, diffuse; 2, early inclusion; 3, late inclusion) that could each have a distinct probability of undergoing apoptosis and dying.

HeLa tet Repressor Experiments

HeLa tet repressor cells were co-transfected with pGW-Httex1-mCherry and pT-REx-Emerald. 24 hr after transfection, the medium was refreshed and supplemented with 1 μ g/mL tetracycline. The cells were imaged for 48 hr with a JuLI-stage live-cell imaging fluorescence microscope (NanoEnTek).

Statistics

The details of the tests are indicated in the figure legends. Non-significant (n.s.) results are defined in the figures for $p > 0.05$. p Values lower than 0.05 are coded as follows: * $p < 0.05$, ** $p < 0.01$, *** $p < 0.001$, **** $p < 0.0001$.

ACCESSION NUMBERS

The accession number for the mass spectrometry data reported in this paper is ProteomeXchange Consortium: PXD005120.

SUPPLEMENTAL INFORMATION

Supplemental Information includes Supplemental Experimental Procedures, seven figures, and two tables and can be found with this article online at <http://dx.doi.org/10.1016/j.celrep.2017.04.029>.

AUTHOR CONTRIBUTIONS

Y.M.R., M.M.T., D.B.A., A.R.O., E.A.N., X.S., C.S.A., N.S.M., and S.W. designed and performed the experiments and analyzed the data. J.N., C.L.P., M.N.B., A.W.P., S.L.G., G.D., M.J.T., J.M.L.M., S.F., M.J.B., J.A.W., D.S., T.B., and G.E.R. designed experiments and/or analyzed data. Y.M.R. and D.M.H. conceived the work. D.M.H. directed the work and prepared the manuscript with contributions from all authors, and all authors contributed to discussions.

ACKNOWLEDGMENTS

This work was funded by a grant to D.M.H. from the Australian Research Council (FT120100039); grants/fellowships from the National Health and Medical Research Council Project to D.M.H. (APP1049458, APP1049459, and APP1102059), J.A.W. (APP1105801), A.W.P. (1044215), and D.B.A. (APP1072476); and a grant to D.M.H. from the Hereditary Disease Foundation. Part of this research was undertaken on the Infrared beamline at the Australian Synchrotron. This research was supported by the Victorian Life Sciences Computation Initiative, an initiative of the Victorian Government, Australia, at its Facility hosted at the University of Melbourne (UOM0017).

Received: October 26, 2016

Revised: March 16, 2017

Accepted: April 10, 2017

Published: May 2, 2017

REFERENCES

Arimoto, K., Fukuda, H., Imajoh-Ohmi, S., Saito, H., and Takekawa, M. (2008). Formation of stress granules inhibits apoptosis by suppressing stress-responsive MAPK pathways. *Nat. Cell Biol.* *10*, 1324–1332.

Arasate, M., Mitra, S., Schweitzer, E.S., Segal, M.R., and Finkbeiner, S. (2004). Inclusion body formation reduces levels of mutant huntingtin and the risk of neuronal death. *Nature* *431*, 805–810.

Bodner, R.A., Outeiro, T.F., Altmann, S., Maxwell, M.M., Cho, S.H., Hyman, B.T., McLean, P.J., Young, A.B., Housman, D.E., and Kazantsev, A.G. (2006). Pharmacological promotion of inclusion formation: a therapeutic

approach for Huntington's and Parkinson's diseases. *Proc. Natl. Acad. Sci. USA* *103*, 4246–4251.

Brandman, O., and Hegde, R.S. (2016). Ribosome-associated protein quality control. *Nat. Struct. Mol. Biol.* *23*, 7–15.

Brandman, O., Stewart-Ornstein, J., Wong, D., Larson, A., Williams, C.C., Li, G.W., Zhou, S., King, D., Shen, P.S., Weibezahn, J., et al. (2012). A ribosome-bound quality control complex triggers degradation of nascent peptides and signals translation stress. *Cell* *151*, 1042–1054.

Caserta, T.M., Smith, A.N., Gultice, A.D., Reedy, M.A., and Brown, T.L. (2003). Q-VD-OPh, a broad spectrum caspase inhibitor with potent antiapoptotic properties. *Apoptosis* *8*, 345–352.

Culver, B.P., Savas, J.N., Park, S.K., Choi, J.H., Zheng, S., Zeittlin, S.O., Yates, J.R., 3rd, and Tanese, N. (2012). Proteomic analysis of wild-type and mutant huntingtin-associated proteins in mouse brains identifies unique interactions and involvement in protein synthesis. *J. Biol. Chem.* *287*, 21599–21614.

Denham, M., Parish, C.L., Leaw, B., Wright, J., Reid, C.A., Petrou, S., Dottori, M., and Thompson, L.H. (2012). Neurons derived from human embryonic stem cells extend long-distance axonal projections through growth along host white matter tracts after intra-cerebral transplantation. *Front. Cell. Neurosci.* *6*, 11.

DiFiglia, M., Sapp, E., Chase, K.O., Davies, S.W., Bates, G.P., Vonsattel, J.P., and Aronin, N. (1997). Aggregation of huntingtin in neuronal intranuclear inclusions and dystrophic neurites in brain. *Science* *277*, 1990–1993.

Gidalevitz, T., Ben-Zvi, A., Ho, K.H., Brignull, H.R., and Morimoto, R.I. (2006). Progressive disruption of cellular protein folding in models of polyglutamine diseases. *Science* *311*, 1471–1474.

Kedersha, N.L., Gupta, M., Li, W., Miller, I., and Anderson, P. (1999). RNA-binding proteins TIA-1 and TIAR link the phosphorylation of eIF-2 alpha to the assembly of mammalian stress granules. *J. Cell Biol.* *147*, 1431–1442.

Kim, H.J., Kim, N.C., Wang, Y.-D., Scarborough, E.A., Moore, J., Diaz, Z., MacLea, K.S., Freibaum, B., Li, S., Molliex, A., et al. (2013). Mutations in prion-like domains in hnRNPA2B1 and hnRNPA1 cause multisystem proteinopathy and ALS. *Nature* *495*, 467–473.

King, M.A., Goemans, C.G., Hafiz, F., Prehn, J.H., Wyttenbach, A., and Tolkovsky, A.M. (2008). Cytoplasmic inclusions of Htt exon1 containing an expanded polyglutamine tract suppress execution of apoptosis in sympathetic neurons. *J. Neurosci.* *28*, 14401–14415.

Korshunov, S.S., Skulachev, V.P., and Starkov, A.A. (1997). High protonic potential actuates a mechanism of production of reactive oxygen species in mitochondria. *FEBS Lett.* *416*, 15–18.

Lajoie, P., and Snapp, E.L. (2010). Formation and toxicity of soluble polyglutamine oligomers in living cells. *PLoS ONE* *5*, e15245.

Lancaster, A.K., Nutter-Upham, A., Lindquist, S., and King, O.D. (2014). PLAAC: a web and command-line application to identify proteins with prion-like amino acid composition. *Bioinformatics* *30*, 2501–2502.

Leitman, J., Ulrich Hartl, F., and Lederkremer, G.Z. (2013). Soluble forms of polyQ-expanded huntingtin rather than large aggregates cause endoplasmic reticulum stress. *Nat. Commun.* *4*, 2753.

Li, Y.R., King, O.D., Shorter, J., and Gitler, A.D. (2013). Stress granules as crucibles of ALS pathogenesis. *J. Cell Biol.* *207*, 361–372.

Lykke-Andersen, J., and Bennett, E.J. (2014). Protecting the proteome: Eukaryotic cotranslational quality control pathways. *J. Cell Biol.* *204*, 467–476.

MacDonald, M.E., Ambrose, C.M., Duyao, M.P., Myers, R.H., Lin, C., Srinidhi, L., Barnes, G., Taylor, S.A., James, M., Groot, N., et al.; The Huntington's Disease Collaborative Research Group (1993). A novel gene containing a trinucleotide repeat that is expanded and unstable on Huntington's disease chromosomes. *Cell* *72*, 971–983.

Nucifora, L.G., Burke, K.A., Feng, X., Arbez, N., Zhu, S., Miller, J., Yang, G., Ratovitski, T., Delannoy, M., Muchowski, P.J., et al. (2012). Identification of novel potentially toxic oligomers formed in vitro from mammalian-derived expanded huntingtin exon-1 protein. *J. Biol. Chem.* *287*, 16017–16028.

Olshina, M.A., Angley, L.M., Ramdzan, Y.M., Tang, J., Bailey, M.F., Hill, A.F., and Hatters, D.M. (2010). Tracking mutant huntingtin aggregation kinetics in

- cells reveals three major populations that include an invariant oligomer pool. *J. Biol. Chem.* **285**, 21807–21816.
- Ormsby, A.R., Ramdhan, Y.M., Mok, Y.-F., Jovanoski, K.D., and Hatters, D.M. (2013). A platform to view huntingtin exon 1 aggregation flux in the cell reveals divergent influences from chaperones hsp40 and hsp70. *J. Biol. Chem.* **288**, 37192–37203.
- Park, S.-H., Kukushkin, Y., Gupta, R., Chen, T., Konagai, A., Hipp, M.S., Hayer-Hartl, M., and Hartl, F.U. (2013). PolyQ proteins interfere with nuclear degradation of cytosolic proteins by sequestering the Sis1p chaperone. *Cell* **154**, 134–145.
- Ramdhan, Y.M., Nisbet, R.M., Miller, J., Finkbeiner, S., Hill, A.F., and Hatters, D.M. (2010). Conformation sensors that distinguish monomeric proteins from oligomers in live cells. *Chem. Biol.* **17**, 371–379.
- Ramdhan, Y.M., Polling, S., Chia, C.P., Ng, I.H., Ormsby, A.R., Croft, N.P., Purcell, A.W., Bogoyevitch, M.A., Ng, D.C., Gleeson, P.A., and Hatters, D.M. (2012). Tracking protein aggregation and mislocalization in cells with flow cytometry. *Nat. Methods* **9**, 467–470.
- Savas, J.N., Ma, B., Deinhardt, K., Culver, B.P., Restituito, S., Wu, L., Belasco, J.G., Chao, M.V., and Tanese, N. (2010). A role for huntington disease protein in dendritic RNA granules. *J. Biol. Chem.* **285**, 13142–13153.
- Schaffar, G., Breuer, P., Boteva, R., Behrends, C., Tsvetkov, N., Strippel, N., Sakahira, H., Siegers, K., Hayer-Hartl, M., and Hartl, F.U. (2004). Cellular toxicity of polyglutamine expansion proteins: mechanism of transcription factor deactivation. *Mol. Cell* **15**, 95–105.
- Scherzinger, E., Lurz, R., Turmaine, M., Mangiarini, L., Hollenbach, B., Hasenbank, R., Bates, G.P., Davies, S.W., Lehrach, H., and Wanker, E.E. (1997). Huntingtin-encoded polyglutamine expansions form amyloid-like protein aggregates *in vitro* and *in vivo*. *Cell* **90**, 549–558.
- Scherzinger, E., Sittler, A., Schweiger, K., Heiser, V., Lurz, R., Hasenbank, R., Bates, G.P., Lehrach, H., and Wanker, E.E. (1999). Self-assembly of polyglutamine-containing huntingtin fragments into amyloid-like fibrils: implications for Huntington's disease pathology. *Proc. Natl. Acad. Sci. USA* **96**, 4604–4609.
- Subach, F.V., Subach, O.M., Gundorov, I.S., Morozova, K.S., Piatkevich, K.D., Cuervo, A.M., and Verkhusha, V.V. (2009). Monomeric fluorescent timers that change color from blue to red report on cellular trafficking. *Nat. Chem. Biol.* **5**, 118–126.
- Takahashi, T., Kikuchi, S., Katada, S., Nagai, Y., Nishizawa, M., and Onodera, O. (2008). Soluble polyglutamine oligomers formed prior to inclusion body formation are cytotoxic. *Hum. Mol. Genet.* **17**, 345–356.
- Takahashi, M., Higuchi, M., Matsuki, H., Yoshita, M., Ohsawa, T., Oie, M., and Fujii, M. (2013). Stress granules inhibit apoptosis by reducing reactive oxygen species production. *Mol. Cell. Biol.* **33**, 815–829.
- Tsvetkov, A.S., Arrasate, M., Barmada, S., Ando, D.M., Sharma, P., Shaby, B.A., and Finkbeiner, S. (2013). Proteostasis of polyglutamine varies among neurons and predicts neurodegeneration. *Nat. Chem. Biol.* **9**, 586–592.
- Vance, C., Rogelj, B., Hortobágyi, T., De Vos, K.J., Nishimura, A.L., Sreedharan, J., Hu, X., Smith, B., Ruddy, D., Wright, P., et al. (2009). Mutations in FUS, an RNA processing protein, cause familial amyotrophic lateral sclerosis type 6. *Science* **323**, 1208–1211.
- Woerner, A.C., Frottin, F., Hornburg, D., Feng, L.R., Meissner, F., Patra, M., Tatzelt, J., Mann, M., Winkhofer, K.F., Hartl, F.U., and Hipp, M.S. (2016). Cytoplasmic protein aggregates interfere with nucleocytoplasmic transport of protein and RNA. *Science* **351**, 173–176.